Inorganic Chemistry

Article

Cite This: Inorg. Chem. 2018, 57, 12050−12055

pubs.acs.org/IC

High Volumetric Hydrogen Adsorption in a Porous Anthracene-Decorated Metal−Organic Framework

Yong Yan,[†] Ivan da Silva,[‡] Alexander J. Blake,[§] Anne Dailly,[∥] Pascal Manuel,[‡] Sihai Yang,*[,†] and Martin Schröder*[,†]

[†]School of Chemistry, University of Manchester, Oxford Road, Manchester M13 9PL, United Kingdom

[‡]ISIS facility, Science and Technology Facilities Council (STFC), Rutherford Appleton Laboratory, Didcot OX11 0QX, United Kingdom

[§]School of Chemistry, University of Nottingham, University Park, Nottingham NG7 2RD, United Kingdom

[∥]Chemical and Environmental Sciences Laboratory, General Motors Corporation, Warren, Michigan 48090, United States

Supporting Information

ABSTRACT: We report an unprecedented ligand-based binding domain for D_2 within a porous metal−organic framework (MOF) material as confirmed by neutron powder diffraction studies of D_2-loaded MFM-132a. A tight pocket of 6 Å diameter is formed by the close packing of three anthracene panels, and it is here rather than the open metal sites where D_2 binds preferentially. As a result, MFM-132a shows exceptional volumetric hydrogen adsorption (52 g L^{-1} at 60 bar and 77 K) and the highest density of adsorbed H_2 within its pores among all the porous materials reported to date under the same conditions. This work points to a new direction for H_2 storage in porous materials using polyaromatic ligand-based sites.

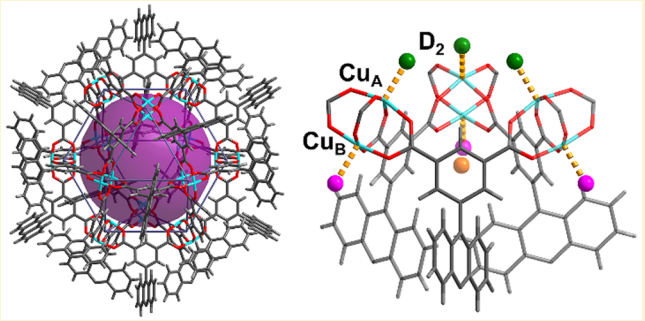

INTRODUCTION

Hydrogen (H_2) is a promising energy carrier for mobile applications due to its abundance and the absence of CO_2 output at the point of use.[1] Although H_2 has a high energy density by mass (120 MJ kg^{-1} vs 44.5 MJ kg^{-1} for gasoline), it has low volumetric energy density because of its volatility at ambient conditions.[2] As a result, a safe and cost-effective storage system with high volumetric capacity is needed to enable the on-board use of H_2. Compared to the state-of-the-art storage techniques based upon liquefaction or high-pressure compression, adsorptive H_2 storage has attracted significant attention.[2−4] Among the wide range of porous materials, such as porous carbons,[5] zeolites,[6] and porous polymers,[7] metal−organic frameworks (MOFs)[8] show great promise for H_2 storage because of their large surface area and tunable and well-defined crystal structures. H_2 adsorption in MOFs follows a physisorption mechanism, where H_2 molecules bind to MOF surfaces through weak dispersive interactions. Thus, MOFs with high surface area usually show high H_2 gravimetric adsorption capacities, albeit at low temperatures. Strategies for enhancing the binding energy between the framework and H_2 are still being actively pursued. These include the synthesis of frameworks containing open metal sites[9] and framework catenation/interpenetration for creating small pore size for enhancing the overlapping potential from opposite pore walls for H_2.[10−12] However, the former is unable to enhance the H_2 adsorption overall because the open metal sites reach saturation quickly at low surface coverage, while the latter often suffers from unpredictable control and significant reduction in the material porosity, and hence reduced total uptake capacity.

Large conjugated aromatic systems can not only provide strong affinity for guest molecules based on specific van der Waals interactions[13] but also significantly enhance the rigidity and stability of the resulting materials.[14] Anthracene has been widely used as a versatile molecular building unit for the construction of a variety of molecular capsules, cages, tubes, and ring structures.[15] The flat, panel-like aromatic system results in cages having enclosed shells, allowing the encapsulated guest molecules to be segregated from the external environment, thus providing unique potential for the encapsulation of guest molecules in these supramolecular hosts.[16] Here, we report an investigation of the adsorption and molecular binding of H_2 in an anthracene-decorated (3, 24)-connected framework (denoted MFM-132). Significantly, desolvated MFM-132a exhibits exceptionally high volumetric H_2 capacity of 52 g L^{-1} at 60 bar and 77 K, among the highest values for porous materials reported under the same conditions. Neutron powder diffraction (NPD) studies of

Received: June 9, 2018
Published: September 19, 2018

DOI: 10.1021/acs.inorgchem.8b01607
Inorg. Chem. 2018, 57, 12050−12055

D_2-loaded MFM-132a reveal that a cleft formed by the anthracene moieties within the pores of MFM-132a is directly responsible for its excellent H_2 adsorption performance by creating specific ligand-based binding domains.

RESULTS AND DISCUSSION

MFM-132 was prepared by the solvothermal reaction of H_6BTAT [H_6BTAT = 5,5′,5″-(benzene-1,3,5-triyltris-(anthracene-10,9-diyl))triisophthalic acid; Figure 1b] and

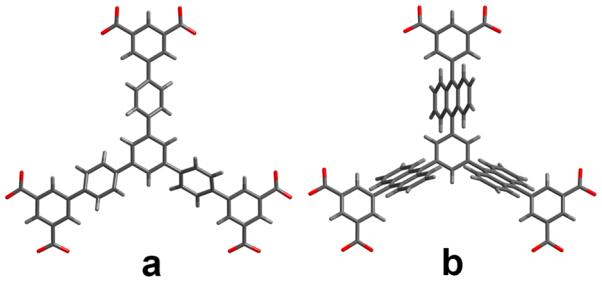

Figure 1. View of the hexacarboxylate linkers containing three isophthalate units in the same plane used to construct MFM-112 and MFM-132: TDBB^{6-}, H_6TDBB = benzene-1,3,5-tris([1,1′-biphenyl]-4-yl-3′,5′-dicarboxylic acid) (a), and BTAT^{6-} with three anthracene rings in the central core (b).

$Cu(NO_3)_2{\cdot}2.5H_2O$ in DMF and isolated as blue-green microcrystalline powder.[17] As-synthesized MFM-132 was solvent-exchanged with acetone and then subjected to thermal evacuation under dynamic vacuum at 100 °C for 16 h to afford the desolvated material MFM-132a as blue-purple powder. Rietveld refinement of the NPD data confirms that MFM-132a has a (3, 24)-connected[18−20] open structure, comprising four types of metal−organic cages (denoted **A**, **B**, **C**, and **D**, Figure 2). Cage **A** (13 Å in diameter), constructed by 12 {Cu_2} paddlewheels and 24 isophthalates from 24 independent BTAT^{6-} units, is heavily shielded by 24 anthracene units from different linkers on the exterior of this cage. In addition, cage **A** also contains 12 open Cu(II) sites internally. With a large number of anthracene panels protruding into the central voids, cages **B** and **C** in MFM-132a show pore sizes of 6.5 and 13 Å (measured by the diameter of the largest sphere which can be fitted into the cavity), respectively. In the void between fused cages **B** and **C** exists the fourth cage, cage **D**, which is a spherical compartment of 10 Å in diameter and has small apertures of 5 Å × 5 Å, enclosed by eight anthracene panels from four linkers and two {Cu_2} paddlewheels. Thus, the cages in MFM-132a show a rich combination of micropores in the range 6−13 Å with varying functionalities, affording a unique pore environment for binding of small guest molecules.

The N_2 isotherm at 77 K for MFM-132a reveals a BET surface area of 2466 $m^2\ g^{-1}$ and total pore volume of 1.06 $cm^3\ g^{-1}$.[17] H_2 sorption isotherms for MFM-132a were recorded using both gravimetric and volumetric methods at 77 K (Figure 3). MFM-132a shows a very high H_2 uptake of 2.83 wt % at 1 bar and 77 K (Table 1). The high H_2 adsorption at low pressure in MFM-132a is comparable to the high-performing Cu(II)-based MOFs UTSA-20[21] and SUT-5.[22] This is due to the combination of the open Cu(II) sites and the geometrically hindered pores with anthracene units in MFM-132a which can provide strong overlapping potential to H_2 molecules.[26] Virial analysis[27] was applied to calculate the coverage-dependent adsorption enthalpies based on the H_2 adsorption isotherms at 77 and 87 K (see Supporting Information). The value of Q_{st} at

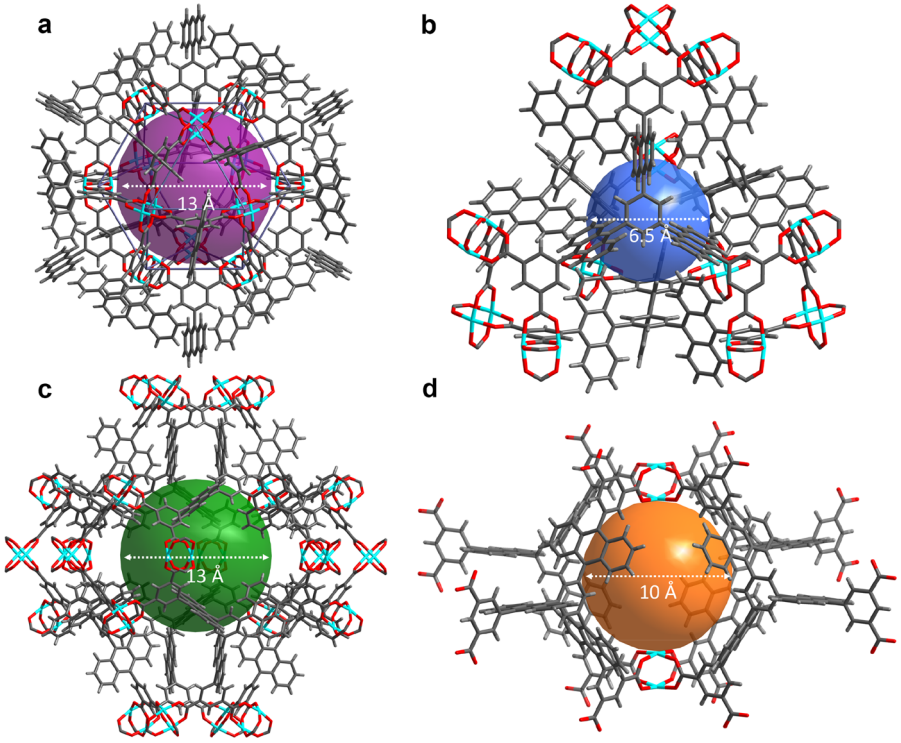

Figure 2. View of the crystal structure of MFM-132a derived from the Rietveld refinement of the NPD data for the bare sample showing four different types of cages: cage **A** (a), cage **B** (b), cage **C** (c), and cage **D** (d). The void within each cage is shown by a colored sphere. Color scheme: C, gray; H, light gray; O, red; Cu, aqua.

DOI: 10.1021/acs.inorgchem.8b01607
Inorg. Chem. 2018, 57, 12050−12055

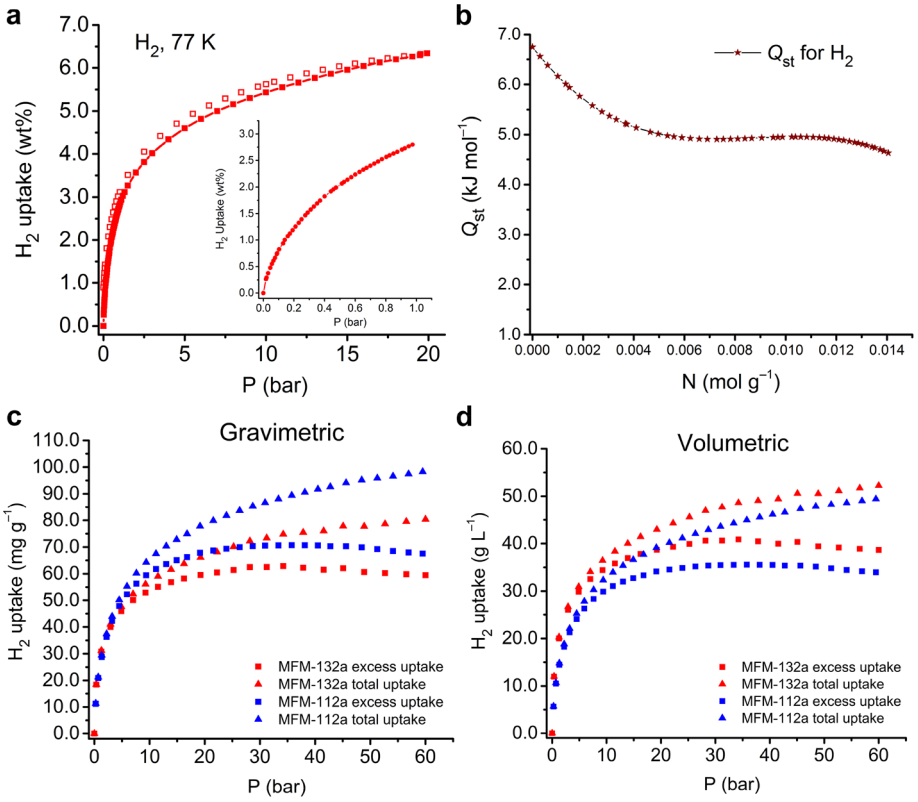

Figure 3. (a) Gravimetric H_2 adsorption isotherm for MFM-132a at 77 K and 20 bar (the insert shows the data in the low-pressure region 0−1 bar). The solid and open squares indicate adsorption and desorption, respectively. (b) Isosteric heat of H_2 adsorption in MFM-132a as a function of H_2 loading. Gravimetric (c) and volumetric (d) comparisons of the high-pressure H_2 adsorption isotherms for MFM-132a and MFM-112a at 77 K.

Table 1. Comparison of the H_2 Adsorption Properties for a Variety of the Best-Behaving MOFs at 77 K

material	BET surface area ($m^2\ g^{-1}$)	pore volume ($cm^3\ g^{-1}$)	crystal density[a] ($g\ cm^{-3}$)	H_2 uptake at 1 bar (wt %)	density of adsorbed H_2 at 1 bar ($g\ cm^{-3}$)	saturated excess H_2 uptake ($mg\ g^{-1}$)	total H_2 uptake ($mg\ g^{-1}$)	total volumetric uptake ($g\ L^{-1}$)	density of adsorbed H_2 at high pressure ($g\ cm^{-3}$)	Q_{st} for H_2 at zero coverage ($kJ\ mol^{-1}$)
MFM-132a	2466	1.06	0.65	2.83	0.026	63	80 (60 bar)	52 (60 bar)	0.075 (60 bar)	6.7
MFM-112a (NOTT-112)[18]	3800	1.62	0.503	2.3	0.014	76.1	98 (60 bar)	49 (60 bar)	0.06 (60 bar)	5.6
NU-100[19b]	6143	2.82	0.279	1.82	0.006	99.5	164 (70 bar)	46 (70 bar)	0.058 (70 bar)	6.1
PCN-66[19a]	4000	1.63	0.45	1.79	0.011	66.5 (45 bar)	96 (60 bar)	43 (60 bar)	0.059 (60 bar)	6.22
PCN-68[19a]	5109	2.13	0.38	1.87	0.009	73.2 (50 bar)	115 (60 bar)	44 (60 bar)	0.054 (60 bar)	6.09
UTSA-20[21]	1156	0.63	0.91	2.9	0.046					
SNU-5[22]	2850	1.0	0.768	2.87	0.028	52	68 (50 bar)	52 (50 bar)	0.068 (50 bar)	11.6
MOF-177[21,22]	4746	1.59	0.427	1.2	0.008	75	106 (60 bar)	45 (60 bar)	0.067 (60 bar)	4.4
MOF-5[23]	3800	1.54	0.59	1.5	0.01	75	92 (60 bar)	60 (60 bar)	0.06 (60 bar)	
MOF-210[24]	6240	3.6	0.25			86	156 (60 bar)	39 (60 bar)	0.043 (60 bar)	

[a]Calculated crystal density based upon the crystal structures with all guest solvent molecules and coordinated H_2O molecules removed from the structural models.

the low loading limit is estimated to be 6.8 kJ mol^{-1}, gradually decreasing to 4.6 kJ mol^{-1} as the H_2 coverage increases to 2.8 wt %. The high-pressure measurement up to 60 bar revealed that the saturated excess H_2 uptake reached 63 mg g^{-1} at 35 bar and 77 K, and the total uptake amounts to 80 mg g^{-1} at 60 bar and 77 K. Although these values are lower than those for MFM-112a (saturated excess uptake of 76.1 mg g^{-1} at 45 bar and 77 K; total uptake of 108 mg g^{-1} at 60 bar and 77 K) due to the reduced surface area and pore volume in MFM-132a, the density of the adsorbed H_2 in MFM-132a reaches a remarkable value of 0.075 g cm^{-3} at 60 bar, the highest observed in a porous material under the same conditions (Table 1). This is because of the geometrically restricted pore system in MFM-132a, which can enable efficient packing of H_2 molecules within the pores.

Volumetric capacity is of critical importance for a given storage system if it is to find practical applications. As shown in Figure 3, although MFM-112a[18] shows comparably higher gravimetric H_2 uptakes than MFM-132a at high pressures (>10 bar), MFM-132a exhibits higher volumetric total H_2 uptake of 52 g L^{-1} at 60 bar and 77 K than that of MFM-112a (49 g L^{-1} under same conditions). It is worth noting that, through this report, the volumetric uptake is derived from the bulk material density on the basis of single crystals, and when the efficiency

DOI: 10.1021/acs.inorgchem.8b01607
Inorg. Chem. 2018, 57, 12050−12055

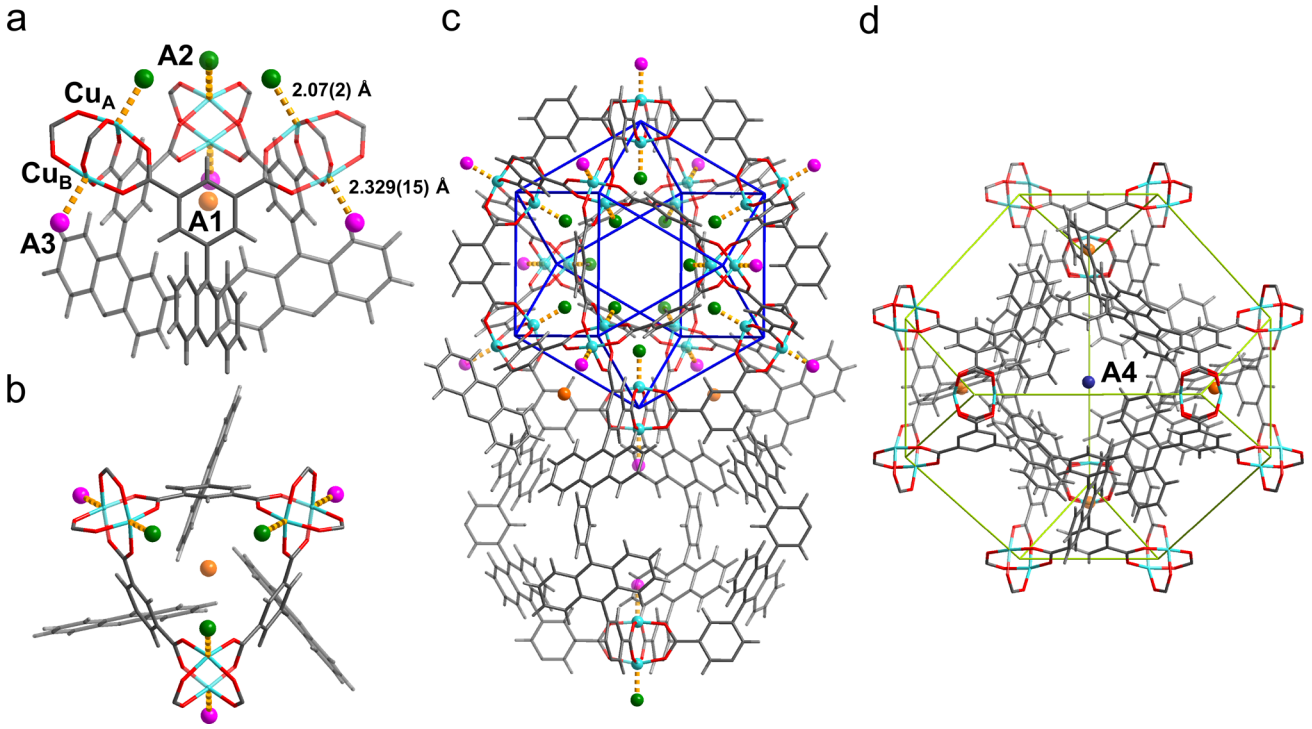

Figure 4. Views of the D_2 adsorption sites revealed by the Rietveld analysis of the NPD data of D_2-loaded MFM-132a. The triangular $\{(Cu_2)_3(isophthalate)_3\}$ window and three anthracene units create a pocket [(a) side view; (b) top view] which accommodates the strongest binding site A1. (c) View of the three distinct adsorption sites found in cages **A** and **D** within MFM-132a. (d) View of the fourth D_2 adsorption site A4 located in the center of the tetrahedral cage. Color scheme: C, gray; H, light gray; O, red; Cu, aqua; site A1, orange; site A2, green; site A3, magenta; site A4, blue.

of powder packing is considered, the uptakes will be reduced accordingly. Significantly, the total volumetric H_2 uptake for MFM-132a is comparable with the best-behaving MOFs to date such as MOF-177,[23,24] anhydrous MOF-5,[25] and NU-100[19b] (Table 1).

In order to evaluate the favored adsorption sites within the cages, *in situ* NPD studies on D_2-loaded MFM-132a at low surface coverage of 0.5 and 1.0 D_2/Cu (1.0 D_2/Cu corresponds to 0.47 wt % of H_2 uptake in MFM-132a) have been performed. Le Bail analyses of the NPD patterns indicated that the unit cell parameters of MFM-132a at different gas loadings remain essentially constant, confirming the structural rigidity of MFM-132a. The positions of adsorbed D_2 molecules were identified in the difference neutron scattering Fourier maps derived from Rietveld refinements of the NPD patterns for both the bare and gas-loaded samples.

At 0.5 D_2/Cu loading, the Rietveld analysis revealed three different D_2 binding sites (Figure 4). Surprisingly, instead of the open Cu(II) site, the first adsorption site for D_2 (A1) was located within the central pocket created by the triangular $\{(Cu_2)_3(isophthalate)_3\}$ window and three anthracene units. Site A1 is 3.260(11) Å away from the closest H atoms on the anthracene units at the bottom of the pocket and is in close contact with the surrounding isophthalate rings at a distance of 3.863(10) Å. This result is in contrast to all other NPD studies on MOFs,[28−33] which uniformly find that the open metal site is the strongest binding site for D_2, with the exception of the rare earth material [Y(BTC)] (BTC^{3-} = 1,3,5-benzenetricarboxylate).[34] The next site to be occupied, A2, is the open Cu(II) site (Cu_A), lying inside the cuboctahedral cage with a close D_2 (centroid)−Cu_A distance of 2.07(2) Å. Interestingly, this is the shortest D_2−Cu distance observed so far for D_2-loaded MOFs,[35] indicating the presence of a binding of H_2 molecules to the open Cu(II) sites. The other Cu(II) ion of the same paddlewheel unit (Cu_B) is identified as the third adsorption site A3, located outside the cuboctahedral cage and pointing toward the center of the cavity of cage **D**. Site A3 shows a longer D_2−Cu distance of 2.329(15) Å, indicating a weaker D_2−Cu binding interaction on the exterior of the cuboctahedral cage. Thus, the Rietveld analysis clearly indicates a difference for D_2 binding between the two Cu(II) sites of the same $\{Cu_2\}$ unit. This D_2 binding preference for the Cu(II) ions inside cage **A** in MFM-132a is consistent with the results of the NPD studies on D_2-loaded MFM-112a with 0.5 D_2/Cu loading,[29] indicating that the specific cuboctahedral configuration of Cu(II) cations can indeed modulate the binding interaction between the open metal site and the D_2 molecule. Incorporation of bulky anthracene groups in MFM-132a affords an enclosed pocket that can accommodate binding site A1, and creates a strong overlapping potential, thereby generating an unprecedented affinity for D_2 that is stronger than at the open Cu(II) sites.

Analysis of the site occupancies from the Rietveld refinements revealed that 54% of site A1 was occupied at the first loading. The other two sites A2 and A3 showed lower occupancies (0.2 and 0.29, respectively) than site A1, confirming the strong affinity for D_2 at site A1. When the loading is increased to 1.0 D_2/Cu, additional D_2 molecules were distributed across the three adsorption sites, and a fourth D_2 binding site A4 (accounting for only 5% of the total adsorbed D_2) was located in the tight pocket of diameter 6.5 Å surrounded by 12 anthracene rings at the center of cage **B**.

The difference in D_2 binding between the two Cu(II) sites from the same $\{Cu_2\}$ paddlewheel was still observed at the

DOI: 10.1021/acs.inorgchem.8b01607
Inorg. Chem. 2018, 57, 12050−12055

higher loading. This is in contrast to the NPD study of MFM-112a with a D_2 loading of 1.0 D_2/Cu, where two Cu(II) sites become equivalent in terms of D2 binding. Thus at higher loading of D_2 in MFM-132a, the Cu_A site shows a D_2−Cu_A distance of 2.302(15) Å which compares with a D_2−Cu_B distance of 2.376(12) Å at 1.0 D_2/Cu loading. This result further confirms the preferential binding with D_2 for the Cu(II) ions inside the cuboctahedral cage in MFM-132a.

CONCLUSIONS

In summary, we report here the adsorption properties of H_2 in an anthracene-functionalized (3, 24)-connected MOF material, MFM-132a, which is assembled by four different types of metal−ligand coordination cages. Despite the presence of a large number of bulky anthracene panels in the framework, MFM-132a still shows moderately high porosity with BET surface area of 2466 $m^2\ g^{-1}$ and pore volume of 1.06 $cm^3\ g^{-1}$, which is attributed to the intrinsic advantage of the (3, 24)-connected network constructed by the tessellation of individual metal−organic polyhedra possessing internal voids. MFM-132a shows remarkable H_2 adsorption over an extended pressure range, and an exceptionally high total volumetric H_2 capacity of 52 g L^{-1} is recorded at 60 bar and 77 K, among the highest values reported for MOFs to date under the same conditions. The high density of adsorbed H_2 confirms that functionalization with large aromatic panels can efficiently pack H_2 within the pores. NPD studies on D_2-loaded MFM-132a confirm the first binding site to be within a tight pocket of 6 Å created by the triangular $\{(Cu_2)_3(isophthalate)_3\}$ window and three anthracene units. Interestingly, this site has significantly higher D_2 occupancy than the subsequently occupied open Cu(II) sites, confirming that the tightly enclosed pocket created solely by organic units can generate binding affinity to D_2. The two Cu(II) sites in the same $\{Cu_2\}$ paddlewheel show discrimination for D_2 binding due to the different chemical environment of these two open metal sites. The Cu(II) ions inside the cuboctahedral cage show a very short D_2(centroid)···Cu distance of 2.07(2) Å. The strategy reported here, based upon the introduction of bulky functional groups on the organic ligand, provides a controllable method to create materials with specific enclosed ligand binding sites for gaseous substrates.

ASSOCIATED CONTENT

Supporting Information

The Supporting Information is available free of charge on the ACS Publications website at DOI: 10.1021/acs.inorgchem.8b01607.

Synthesis, gas adsorption measurements, powder X-ray diffraction, neutron powder diffraction patterns, and Rietveld refinement results (PDF)

Accession Codes

CCDC 1506079−1506080 contain the supplementary crystallographic data for this paper. These data can be obtained free of charge via www.ccdc.cam.ac.uk/data_request/cif, or by emailing data_request@ccdc.cam.ac.uk, or by contacting The Cambridge Crystallographic Data Centre, 12 Union Road, Cambridge CB2 1EZ, UK; fax: +44 1223 336033.

AUTHOR INFORMATION

Corresponding Authors

*E-mail: Sihai.Yang@manchester.ac.uk.

*E-mail: M.Schroder@manchester.ac.uk.

ORCID

Alexander J. Blake: 0000-0003-2257-8332

Sihai Yang: 0000-0002-1111-9272

Martin Schröder: 0000-0001-6992-0700

Notes

The authors declare no competing financial interest.

ACKNOWLEDGMENTS

We thank the EPSRC (EP/I011870), ERC (AdG 742041), and the University of Manchester for funding. We are grateful to STFC and the ISIS Neutron Facility for access to Beamline WISH.

REFERENCES

(1) Schlapbach, L.; Züttel, A. Hydrogen-storage materials for mobile applications. *Nature* **2001**, *414*, 353−358.

(2) van den Berg, A. W. C.; Areán, C. O. Materials for hydrogen storage: current research trends and perspectives. *Chem. Commun.* **2008**, *6*, 668−681.

(3) DOE Office of Energy Efficiency and Renewable Energy Hydrogen, Fuel Cells & Infrastructure Technologies Program Multi-Year Research, Development and Demonstration Plan. Available at https://www.hydrogen.energy.gov, accessed 25 July 2018.

(4) Eberle, U.; Felderhoff, M.; Schüth, F. Chemical and physical solutions for hydrogen storage. *Angew. Chem., Int. Ed.* **2009**, *48*, 6608−6630.

(5) (a) Sevilla, M.; Mokaya, R. Energy storage applications of activated carbons: supercapacitors and hydrogen storage. *Energy Environ. Sci.* **2014**, *7*, 1250−1280. (b) Masika, E.; Mokaya, R. Exceptional gravimetric and volumetric hydrogen storage for densified zeolite templated carbons with high mechanical stability. *Energy Environ. Sci.* **2014**, *7*, 427−434.

(6) Weitkamp, J.; Fritz, M.; Ernst, S. Zeolites as media for hydrogen storage. *Int. J. Hydrogen Energy* **1995**, *20*, 967−970.

(7) (a) Germain, J.; Frechet, J. M. J.; Svec, F. Nanoporous polymers for hydrogen storage. *Small* **2009**, *5*, 1098−1111. (b) Wood, C. D.; Tan, B.; Trewin, A.; Niu, H.; Bradshaw, D.; Rosseinsky, M. J.; Khimyak, Y. Z.; Campbell, N. L.; Kirk, R.; Stöckel, E.; Cooper, A. I. Hydrogen storage in microporous hypercrosslinked organic polymer networks. *Chem. Mater.* **2007**, *19*, 2034−2048.

(8) (a) Lin, X.; Jia, J.; Hubberstey, P.; Schröder, M.; Champness, N. R. Hydrogen storage in metal−organic frameworks. *CrystEngComm* **2007**, *9*, 438−448. (b) Sculley, J.; Yuan, D.; Zhou, H.-C. The current status of hydrogen storage in metal−organic frameworks—updated. *Energy Environ. Sci.* **2011**, *4*, 2721−2735.

(9) (a) Dincă, M.; Long, J. R. Hydrogen storage in microporous metal-organic frameworks with exposed metal sites. *Angew. Chem., Int. Ed.* **2008**, *47*, 6766−6779. (b) Zhou, W.; Wu, H.; Yildirim, T. Enhanced H_2 adsorption in isostructural metal−organic frameworks with open metal sites: strong dependence of the binding strength on metal ions. *J. Am. Chem. Soc.* **2008**, *130*, 15268−15269. (c) Levine, D. J.; Runčevski, T.; Kapelewski, M. T.; Keitz, B. K.; Oktawiec, J.; Reed, D. A.; Mason, J. A.; Jiang, H. Z. H.; Colwell, K. A.; Legendre, C. M.; FitzGerald, S. A.; Long, J. R. Olsalazine-based metal−organic frameworks as biocompatible platforms for H_2 adsorption and drug delivery. *J. Am. Chem. Soc.* **2016**, *138*, 10143−10150. (d) Gygi, D.; Bloch, E. D.; Mason, J. A.; Hudson, M. R.; Gonzalez, M. I.; Siegelman, R. L.; Darwish, T. A.; Queen, W. L.; Brown, C. M.; Long, J. R. Hydrogen storage in the expanded pore metal−organic frameworks M_2(dobpdc) (M = Mg, Mn, Fe, Co, Ni, Zn). *Chem. Mater.* **2016**, *28*, 1128−1138.

(10) (a) Sun, D.; Ma, S.; Ke, Y.; Collins, D. J.; Zhou, H.-C. An interweaving MOF with high hydrogen uptake. *J. Am. Chem. Soc.* **2006**, *128*, 3896−3897. (b) Jiang, H.-L.; Makal, T. A.; Zhou, H.-C. Interpenetration control in metal−organic frameworks for functional applications. *Coord. Chem. Rev.* **2013**, *257*, 2232−2249.

DOI: 10.1021/acs.inorgchem.8b01607
Inorg. Chem. 2018, 57, 12050−12055

(11) Murray, L. J.; Dincă, M.; Long, J. R. Hydrogen storage in metal−organic frameworks. *Chem. Soc. Rev.* **2009**, *38*, 1294−1314.
(12) Suh, M. P.; Park, H. J.; Prasad, T. K.; Lim, D.-W. Hydrogen storage in metal−organic frameworks. *Chem. Rev.* **2012**, *112*, 782−835.
(13) Yang, S.; Lin, X.; Dailly, A.; Blake, A. J.; Champness, N. R.; Hubberstey, P.; Schröder, M. Enhancement of H_2 adsorption in coordination framework materials by use of ligand curvature. *Chem. - Eur. J.* **2009**, *15*, 4829−4835.
(14) Bichoutskaia, E.; Suyetin, M.; Bound, M.; Yan, Y.; Schröder, M. Methane adsorption in metal−organic frameworks containing nanographene linkers: a computational study. *J. Phys. Chem. C* **2014**, *118*, 15573−15580.
(15) Yoshizawa, M.; Klosterman, J. K. Molecular architectures of multi-anthracene assemblies. *Chem. Soc. Rev.* **2014**, *43*, 1885−1898.
(16) Kishi, N.; Li, Z.; Yoza, K.; Akita, M.; Yoshizawa, M. An M_2L_4 molecular capsule with an anthracene shell: encapsulation of large guests up to 1 nm. *J. Am. Chem. Soc.* **2011**, *133*, 11438−11441.
(17) Yan, Y.; Kolokolov, D. I.; da Silva, I.; Stepanov, A. G.; Blake, A. J.; Dailly, A.; Manuel, P.; Tang, C. C.; Yang, S.; Schröder, M. Porous metal−organic polyhedral frameworks with optimal molecular dynamics and pore geometry for methane storage. *J. Am. Chem. Soc.* **2017**, *139*, 13349−13360.
(18) (a) Yan, Y.; Yang, S.; Blake, A. J.; Schröder, M. Studies on metal−organic frameworks of Cu(II) with isophthalate linkers for hydrogen storage. *Acc. Chem. Res.* **2014**, *47*, 296−307. (b) Yan, Y.; Lin, X.; Yang, S.; Blake, A. J.; Dailly, A.; Champness, N. R.; Hubberstey, P.; Schröder, M. Exceptionally high H_2 storage by a metal−organic polyhedral framework. *Chem. Commun.* **2009**, *9*, 1025−1027.
(19) (a) Yuan, D.; Zhao, D.; Sun, D.; Zhou, H.-C. An isoreticular series of metal−organic frameworks with dendritic hexacarboxylate ligands and exceptionally high gas-uptake capacity. *Angew. Chem., Int. Ed.* **2010**, *49*, 5357−5361. (b) Farha, O. K.; Ozgur, Y. A.; Eryazici, I.; Malliakas, C. D.; Hauser, B. G.; Kanatzidis, M. G.; Nguyen, S. T.; Snurr, R. Q.; Hupp, J. T. *De novo* synthesis of a metal−organic framework material featuring ultrahigh surface area and gas storage capacities. *Nat. Chem.* **2010**, *2*, 944−948. (c) Zheng, B.; Bai, J.; Duan, J.; Wojtas, L.; Zaworotko, M. J. Enhanced CO_2 binding affinity of a high-uptake *rht*-type metal−organic framework decorated with acylamide groups. *J. Am. Chem. Soc.* **2011**, *133*, 748−751. (d) Eubank, J. F.; Nouar, F.; Luebke, R.; Cairns, A. J.; Wojtas, L.; Alkordi, M.; Bousquet, T.; Hight, M. R.; Eckert, J.; Embs, J. P.; Georgiev, P. A.; Eddaoudi, M. On demand: the singular rht net, an ideal blueprint for the construction of a metal−organic framework (MOF) Platform. *Angew. Chem., Int. Ed.* **2012**, *51*, 10099−10103.
(20) (a) Yan, Y.; Blake, A. J.; Lewis, W.; Barnett, S. A.; Dailly, A.; Champness, N. R.; Schröder, M. Modifying cage structures in metal−organic polyhedral frameworks for H_2 storage. *Chem. - Eur. J.* **2011**, *17*, 11162−11170. (b) Yan, Y.; Suyetin, M.; Bichoutskaia, E.; Blake, A. J.; Allan, D. R.; Barnett, S. A.; Schröder, M. Modulating the packing of $[Cu_{24}(isophthalate)_{24}]$ cuboctahedra in a triazole-containing metal−organic polyhedral framework. *Chem. Sci.* **2013**, *4*, 1731−1736. (c) Wilmer, C. E.; Farha, O. K.; Yildirim, T.; Eryazici, I.; Krungleviciute, V.; Sarjeant, A. A.; Snurr, R. Q.; Hupp, J. T. Gram-scale, high-yield synthesis of a robust metal−organic framework for storing methane and other gases. *Energy Environ. Sci.* **2013**, *6*, 1158−1163.
(21) Guo, Z.; Wu, H.; Srinivas, G.; Zhou, Y.; Xiang, S.; Chen, Z.; Yang, Y.; Zhou, W.; O'Keeffe, M.; Chen, B. A metal−organic framework with optimized open metal sites and pore spaces for high methane storage at room temperature. *Angew. Chem., Int. Ed.* **2011**, *50*, 3178−3181.
(22) Lee, Y.-G.; Moon, H. R.; Cheon, Y. E.; Suh, M. P. A comparison of the H_2 sorption capacities of isostructural metal−organic frameworks with and without accessible metal sites: $[\{Zn_2(abtc)(dmf)_2\}_3]$ and $[\{Cu_2(abtc)(dmf)_2\}_3]$ versus $[\{Cu_2(abtc)\}_3]$. *Angew. Chem., Int. Ed.* **2008**, *47*, 7741−7745.
(23) Rowsell, J. L. C.; Millward, A. R.; Park, K. S.; Yaghi, O. M. Hydrogen sorption in functionalized metal−organic frameworks. *J. Am. Chem. Soc.* **2004**, *126*, 5666−5667.
(24) Furukawa, H.; Miller, M. A.; Yaghi, O. M. Independent verification of the saturation hydrogen uptake in MOF-177 and establishment of a benchmark for hydrogen adsorption in metal−organic frameworks. *J. Mater. Chem.* **2007**, *17*, 3197−3204.
(25) Kaye, S. S.; Dailly, A.; Yaghi, O. M.; Long, J. R. Impact of preparation and handling on the hydrogen storage properties of Zn_4O(1,4-benzenedicarboxylate)$_3$ (MOF-5). *J. Am. Chem. Soc.* **2007**, *129*, 14176−14177.
(26) Furukawa, H.; Ko, N.; Go, Y. B.; Aratani, N.; Choi, S. B.; Choi, E.; Yazaydin, A. Ö.; Snurr, R. Q.; O'Keeffe, M.; Kim, J.; Yaghi, O. M. Ultrahigh porosity in metal−organic frameworks. *Science* **2010**, *329*, 424−428.
(27) Czepirski, L.; Jagiełło, J. Virial-type thermal equation of gas−solid adsorption. *Chem. Eng. Sci.* **1989**, *44*, 797−801.
(28) Peterson, V. K.; Liu, Y.; Brown, C. M.; Kepert, C. J. Neutron powder diffraction study of D_2 sorption in Cu_3(1,3,5-benzenetricarboxylate)$_2$. *J. Am. Chem. Soc.* **2006**, *128*, 15578−15579.
(29) Yan, Y.; Telepeni, I.; Yang, S.; Lin, X.; Kockelmann, W.; Dailly, A.; Blake, A. J.; Lewis, W.; Walker, G. S.; Allan, D. R.; Barnett, S. A.; Champness, N. R.; Schröder, M. Metal−organic polyhedral frameworks: high H_2 adsorption capacities and neutron powder diffraction studies. *J. Am. Chem. Soc.* **2010**, *132*, 4092−4094.
(30) Lin, X.; Telepeni, I.; Blake, A. J.; Dailly, A.; Brown, C. M.; Simmons, J. M.; Zoppi, M.; Walker, G. S.; Thomas, K. T.; Mays, T. J.; Hubberstey, P.; Champness, N. R.; Schröder, M. High capacity hydrogen adsorption in Cu(II) tetracarboxylate framework materials: the role of pore size, ligand functionalization, and exposed metal sites. *J. Am. Chem. Soc.* **2009**, *131*, 2159−2171.
(31) Dincă, M.; Dailly, A.; Liu, Y.; Brown, C. M.; Neumann, D. A.; Long, J. R. Hydrogen storage in a microporous metal−organic framework with exposed Mn^{2+} coordination sites. *J. Am. Chem. Soc.* **2006**, *128*, 16876−16883.
(32) Kapelewski, M. T.; Geier, S. J.; Hudson, M. R.; Stück, D.; Mason, J. A.; Nelson, J. N.; Xiao, D. J.; Hulvey, Z.; Gilmour, E.; FitzGerald, S. A.; Head-Gordon, M.; Brown, C. M.; Long, J. R. M_2(m-dobdc) (M = Mg, Mn, Fe, Co, Ni) metal−organic frameworks exhibiting increased charge density and enhanced H_2 binding at the open metal sites. *J. Am. Chem. Soc.* **2014**, *136*, 12119−12129.
(33) Bloch, E. D.; Queen, W. L.; Hudson, M. R.; Mason, J. A.; Xiao, D. J.; Murray, L. J.; Flacau, R.; Brown, C. M.; Long, J. R. Hydrogen storage and selective, reversible O_2 adsorption in a metal−organic framework with open chromium(II) sites. *Angew. Chem., Int. Ed.* **2016**, *55*, 8605−8609.
(34) Luo, J.; Xu, H.; Liu, Y.; Zhao, Y.; Daemen, L. L.; Brown, C.; Timofeeva, T. V.; Ma, S.; Zhou, H.-C. Hydrogen adsorption in a highly stable porous rare-earth metal−organic framework: sorption properties and neutron diffraction studies. *J. Am. Chem. Soc.* **2008**, *130*, 9626−9627.
(35) Sumida, K.; Horike, S.; Kaye, S. S.; Herm, Z. R.; Queen, W. L.; Brown, C. M.; Grandjean, F.; Long, G. J.; Dailly, A.; Long, J. R. Hydrogen storage and carbon dioxide capture in an iron-based sodalite-type metal−organic framework (Fe-BTT) discovered *via* high-throughput methods. *Chem. Sci.* **2010**, *1*, 184−191.

DOI: 10.1021/acs.inorgchem.8b01607
Inorg. Chem. 2018, 57, 12050−12055